Journal of Hazardous Materials 190 (2011) 700–706

Contents lists available at ScienceDirect

Journal of Hazardous Materials

journal homepage: www.elsevier.com/locate/jhazmat

Photocatalytic activity of novel AgBr/WO_3 composite photocatalyst under visible light irradiation for methyl orange degradation

Jing Cao*, Bangde Luo, Haili Lin, Shifu Chen

School of Chemistry and Material Science, Huaibei Normal University, 100 Dongshan Road, Huaibei 235000, China

ARTICLE INFO

Article history:
Received 7 August 2010
Received in revised form 6 March 2011
Accepted 29 March 2011
Available online 8 April 2011

Keywords:
AgBr/WO_3
Photocatalyst
Visible light photocatalysis
Composite
Methyl orange

ABSTRACT

A novel AgBr/WO_3 composite photocatalyst was synthesized by loading AgBr on WO_3 substrate via deposition–precipitation method and characterized by XRD, SEM and DRS. The as-prepared AgBr/WO_3 was composed of monoclinic WO_3 substrate and face-centered cubic AgBr nanoparticles with crystalline sizes less than 56.8 nm. AgBr/WO_3 had absorption edge at about 470 nm in the visible light region. The optical AgBr content in AgBr/WO_3 was 0.30:1 (Ag/W) at the corresponding apparent rate, k_{app}, of 0.0160 min^{-1} for MO degradation. The highest k_{app} was 0.0216 min^{-1} for 4 g/L catalyst. The •OH acted as active species. Addition of H_2O_2 within 0.020 mmol/L can efficiently trap electrons to generate more •OH and further improved photocatalytic activity of AgBr/WO_3.

1. Introduction

In recent years, numerous efforts have been made to develop visible light driven photocatalysts in order to utilize solar energy efficiently [1–6]. Generally, there are two ways to exploit visible light photocatalysts. One way is to extend the light absorption of common TiO_2 from ultraviolet region to the visible light area by doping impurity elements [7–9], dye sensitization [10], noble metal deposition, such as Ag [11], Pt [12]. The other way is to develop new materials, such as $BiVO_4$, $CaIn_2O_4$, TaON, $BiTaO_4$, with visible light photocatalytic activity [13–16]. However, there are still some drawbacks hindering their practical applications, which make it necessary to design new photocatalysts to meet the requirements of future application.

Silver halide AgX (X = Cl, Br, I) is an important photosensitive material extensively used in photography technology. Under visible light AgBr can absorb photons to generate electron-hole pairs. Thus AgBr may be used as a potential visible light photocatalyst [17]. But photodecomposition of pure AgBr reduces its activity in practical applications. Recently, a great deal of attention has been paid to certain variety of AgX based composite photocatalysts. The general way is loading AgX grains as visible light active components on different substrates, like SiO_2 [18], TiO_2 [19–26], Al_2O_3 [27–29], Al-MCM-41 [30], Y-zeolite [31], Fe_3O_4 [32], BiOI [33], H_2WO_4 [34,35] and Bi_2WO_6 [36,37] to form composite catalysts. Such supported AgX catalysts can display high photocatalytic activity and also maintain optical stability to some extent. The probable reason is that electron-hole pairs are efficiently separated by the metal silver on the surface of the catalysts [36] or the heterojunction structure is formed between AgX and substrate [34].

Therefore, construction of composites with appropriate energy band structures may therefore achieve the high efficiency and stability for AgX based composite photocatalysts. Based on the band gaps of WO_3 (2.71 eV) [38] and AgBr (2.50 eV) [39], the conduction band (CB) lower and valence band (VB) higher values of WO_3 are 0.747 eV, 3.457 eV and those of AgBr are 0.058 eV, 2.558 eV, respectively, as calculated using the method described by Zhang et al. [40]. It suggests that they have matched energy band structures, which makes it feasible to construct a novel AgBr/WO_3 composite catalyst that may display good separation ability of electron-hole pairs.

In the present work, AgBr/WO_3 composite catalyst was synthesized by directly loading AgBr on WO_3 substrate with simple deposition–precipitation method under a moderate condition. The photocatalytic activities of AgBr/WO_3 were evaluated with methyl orange (MO) as model contaminant under visible light irradiation ($\lambda > 420$ nm). The aims of the experiment were to study the effects of AgBr content in AgBr/WO_3, catalyst amount, initial dye concentration as well as light intensity on the photocatalytic activities of AgBr/WO_3. Moreover, the stability of synthesized AgBr/WO_3 was investigated through successive 7 cycles of experiments. In addition, the mechanism of MO degradation by using AgBr/WO_3 were discussed on the basis of the fluorescence emission spectra of electron-hole recombination and active species •OH, respectively.

* Corresponding author. Tel.: +86 561 3806611; fax: +86 561 3803141.
E-mail addresses: caojing@mail.ipc.ac.cn, chshifu@chnu.edu.cn (J. Cao).

0304-3894/$ – see front matter © 2011 Elsevier B.V. All rights reserved.
doi:10.1016/j.jhazmat.2011.03.112

2. Experimental

2.1. Chemicals and materials

WO_3, $AgNO_3$, NaBr, methyl orange (MO), NH_4OH (25 wt% NH_3), H_2O_2, $BaSO_4$, NaOH and terephthalic acid (TA) are of analytical purity from Sinopharm Chemical Reagent Co., Ltd. and used for the experiment without further purification. Deionized water was used throughout this study.

2.2. Preparation of catalyst

AgBr/WO_3 was prepared by the deposition–precipitation method in a dark room. A 40 W red light with a red color filter (PJ brand, Westingarea Corporation, China) was used to facilitate the experimental manipulation and prevent the decomposition of AgBr. In a typical procedure, 1 g of WO_3 dispersed in 500 mL of deionized water was placed in a 1000 mL Pyrex glass beaker, and the suspension was sonicated for 30 min. Then, 0.072 g of $AgNO_3$ in 0.80 mL of NH_4OH (25 wt% NH_3) was added to the WO_3 suspension and stirred magnetically for 30 min. Subsequently 0.044 g of NaBr in 50 mL of deionized water was quickly added to the mixture. The resulting suspension was vigorously stirred for 10 h. The whole reaction process was kept at room temperature. Finally the product was filtered, washed with deionized water for several times, and dried at 65 °C for 24 h. Yellow AgBr/WO_3–0.10 with theoretical Ag/W molar ratio of 0.10:1 was obtained. In a similar manner, AgBr/WO_3 photocatalysts with different AgBr contents were respectively obtained and defined as TA-0.05, TB-0.10, TC-0.15, TD-0.20, TE-0.25, TF-0.30 and TG-0.40.

2.3. Characterization of catalyst

X-ray diffraction (XRD) measurements were carried out at room temperature using a BRUKER D8 ADVANCE X-ray powder diffractometer with Cu Kα radiation (λ = 1.5406 Å) and a scanning speed of 10°/min. The accelerating voltage and emission current were 40 kV and 30 mA, respectively [41].

JEOL JSM-6610LV scanning electron microscopy (SEM) with 20 kV scanning voltages was employed to observe the morphologies of as-prepared catalysts [42].

UV–vis diffuse reflectance spectroscopy (DRS) measurements were carried out using a Pgeneral TU-1901 UV–vis spectrophotometer equipped with an integrating sphere attachment. The analysis range was from 300 to 650 nm, and $BaSO_4$ was used as a reflectance standard [24].

The band gap energy of the prepared catalysts can be calculated by the following formula [1,43]:

$$\alpha h\nu = A(h\nu - E_g)^{n/2} \quad (1)$$

where α, ν, E_g and A are absorption coefficient, light frequency, band gap energy, and a constant, respectively. Among them, n is determined by the type of optical transition of a semiconductor ($n = 1$ for direct transition and $n = 4$ for indirect transition). The values of n for AgBr and WO_3 are 4 [33] and 1 [38], respectively.

Fluorescence emission spectra were recorded on a JASCO FP-6500 type fluorescence spectrophotometer with 260 nm excited source over a wavelength range of 400–600 nm [44].

2.4. Evaluation of photocatalytic activities of AgBr/WO_3 under visible light

The photocatalytic activities of AgBr/WO_3 were evaluated by photodegradation of MO under irradiation of visible light (λ > 420 nm). The experimental apparatus consists of two parts [45]. The first part is an annular quartz tube. A 500 W Xe lamp (Institute of Electric Light Source, Beijing) with a maximum emission at about 470 nm as visible light source that is laid in the empty chamber of the annular quartz tube. The wavelength of the visible light is controlled through a 420 nm cutoff filter (Instrument Company of Nantong, China). The running water passes through an inner thimble of the annular quartz tube to immediately remove the heat released from the lamp. The second part is a 100 mL unsealed beaker of 5 cm diameter as the reaction vessel.

Experimental procedure are as follows: At ambient temperature, 50 mL of the reaction suspension containing 0.10 g AgBr/WO_3 catalyst and MO (10 mg/L, neutral condition) was put in the 100 mL beaker, and a magnetron was used to stir the reaction solution. The distance between the light source and the surface of the reaction solution is 11 cm. The light intensity was measured by a light meter (JD-3, Shanghai) and was fixed at 6000 lx. Prior to the irradiation, the suspension was magnetically stirred in the dark for 20 min. At the given time intervals, about 5 mL of the suspension was taken from the reaction suspension, centrifuged at 4000 rpm for 30 min and filtered through a 0.2 μm Millipore filter to remove the catalyst particles. The filtrate was then analyzed using 722 s spectrophotometer (Shanghai Precision and Scientific Instrument Company). The MO concentration was determined from the absorbance at a wavelength of 464 nm with deionized water as a reference sample.

According to the Langmuir–Hinshelwood (L–H) kinetics model [43,46–48], the photocatalytic process of MO can be expressed as the following apparent pseudo-first-order kinetics equation [46]:

$$\ln \frac{C_0}{C} = k_{app}t \quad (2)$$

where k_{app} is the apparent pseudo-first-order rate constant (min^{-1}), C is MO concentration in aqueous solution at time t (mg/L), C_0 is initial MO concentration (mg/L).

2.5. Stability of catalyst

The stability of AgBr/WO_3 was investigated by successive 7 cycles of experiments. The catalyst amount, dye amount, irradiation time and light intensity were 2.0 g/L, 50 mL of MO (10 mg/L, neutral condition), 1 h and 6000 lx, respectively, for each cycle. After 1 h irradiation of visible light, all the suspension was taken from the beaker, centrifuged at 4000 rpm for 30 min to remove the bulk solution. Then the solid catalyst was washed with deionized water and further centrifuged for 3 times, respectively. Finally the solid catalyst was dried at 65 °C for 24 h for the next run.

2.6. Analysis of hydroxyl radicals (•OH)

The formed •OH radicals on the surface of AgBr/WO_3 illuminated by visible light were detected by photoluminescence (PL) technique with terephthalic acid (TA) as a probe molecule in this study. The principle is that TA readily reacts with •OH to produce highly fluorescent product, 2-hydroxyterephthalic acid (HTA). The intensity of the PL peak of HTA is in proportion to the amount of •OH radicals produced in water [49,50]. This technique has been extensively used in many fields for the detection of •OH generated in water, such as in radiation chemistry, sonochemistry and biochemistry [51–53]. This method relies on the PL signal at 425 nm of the hydroxylation of TA with •OH generated at the water/catalyst interface.

Experimental procedures are as follows: 0.1 g of AgBr/WO_3 powder sample was dispersed in a 20 mL of the 5×10^{-4} mol/L TA aqueous solution with a concentration of 2×10^{-3} mol/L NaOH at room temperature. The same condition was applied to irradiate the above suspension as for the photocatalytic activity evaluation of catalysts (in Section 2.4). After 1 h irradiation of visible light,

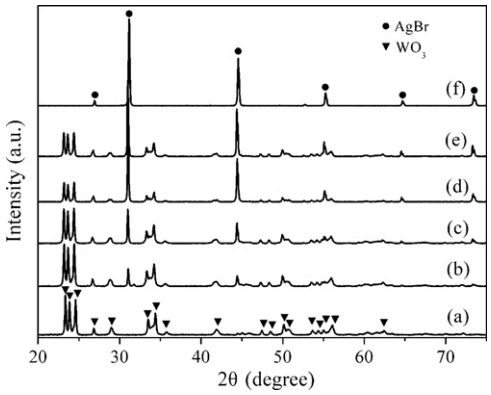

Fig. 1. XRD patterns of (a) WO_3, (b) TB-0.10, (c) TD-0.20, (d) TF-0.30, (e) TG-0.40 and (f) AgBr.

about 5 mL of the suspension was taken from the reaction suspension, centrifuged at 4000 rpm for 30 min and filtered through a 0.2 μm Millipore filter to remove the particles. The filtrate was then analyzed using JASCO FP-6500 fluorescence spectrophotometer to measure the PL intensity at 425 nm induced with 315 nm excitation.

3. Results and discussion

3.1. Characterization of AgBr/WO_3 photocatalysts

In order to confirm the crystalline structure of prepared AgBr/WO_3, powder XRD study was carried out. Fig. 1 shows the XRD patterns of fresh AgBr/WO_3 with different AgBr contents. The patterns show that WO_3 substrate was monoclinic crystal (JCPDS 075-2072) and AgBr was of face-centered cubic structure (JCPDS 06-0438). WO_3 and AgBr coexisted in the AgBr/WO_3 catalysts. With increasing AgBr content, the intensities of diffraction peaks of AgBr increased whereas those of WO_3 decreased simultaneously. The average crystalline sizes of AgBr on the surface of WO_3 were calculated to be 37.2 nm (catalyst TB-0.10), 47.7 nm (catalyst TD-0.20), 50.6 nm (catalyst TF-0.30), 56.8 nm (catalyst TG-0.40) and 58.4 nm (pure AgBr), respectively, by using Scherrer equation [54].

$$L = \frac{K\lambda}{\beta \cos \theta_B} \quad (3)$$

where L is taken as crystalline size, K is a constant equals to 0.9, λ is 1.5406 Å, β is the FWHM measured in radians on the 2θ scale, θ_B is the Bragg angle for the diffraction peaks.

The morphology of AgBr/WO_3 was characterized by SEM and the results are displayed in Fig. 2. From Fig. 2(a), the particle sizes of WO_3 substrates were in the range of 1–6 μm. The loaded AgBr nanoparticles on the surface of WO_3 had irregular shapes with particle size 200–600 nm, as shown in Fig. 2(b).

Fig. 3 shows the UV–vis diffuse reflectance spectra of pure WO_3, AgBr and AgBr/WO_3. It is shown that WO_3, AgBr and AgBr/WO_3 all exhibited absorption in the visible light region, among which the absorption edge of AgBr/WO_3 (470 nm) was lower than that of pure AgBr (485 nm) and WO_3 (491 nm). This also suggests that the crystalline size of AgBr supported on the surface of WO_3 is smaller than that of pure AgBr in this study [17].

According to Eq. (1), E_g of AgBr was determined from the plot of $(\alpha h\nu)^{1/2}$ versus energy ($h\nu$) (Fig. 4a). From the tangent line of the curve, extrapolated to the $h\nu$ axis intercept, E_g of AgBr was found to be 2.46 eV. Similarly, E_g of WO_3 was 2.68 eV (Fig. 4b).

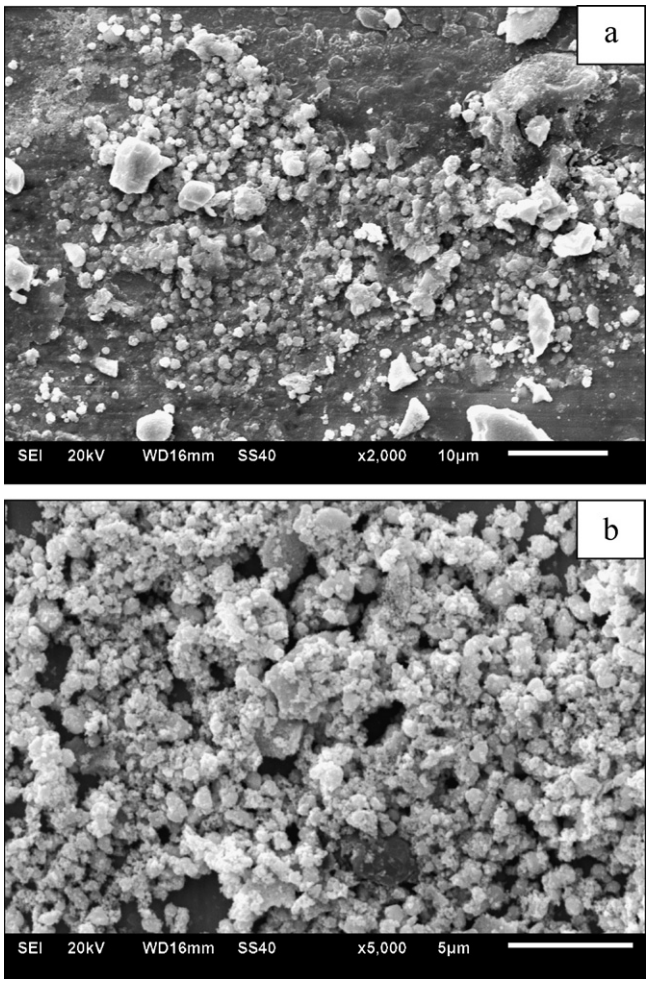

Fig. 2. SEM images of (a) WO_3 and (b) AgBr/WO_3 (catalyst TD-0.20).

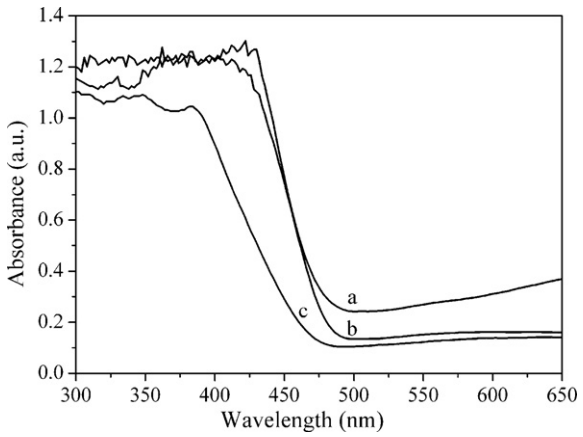

Fig. 3. DRS spectra of (a) WO_3, (b) AgBr and (c) AgBr/WO_3 (catalyst TB-0.10).

3.2. Photocatalytic activities of AgBr/WO_3

3.2.1. Effect of AgBr content

The degradation of MO in the presence of AgBr/WO_3 with different AgBr contents was measured and the results are shown in Fig. 5. Under visible light, WO_3 as a reference had no photocatalytic activity for MO though it can absorb visible light. The photocatalytic activity of AgBr/WO_3 increased remarkably with increasing AgBr content, but at the higher AgBr level the catalyst photocatalytic

Table 1
Effects of AgBr content, catalyst amount, initial MO concentration, light intensity and H_2O_2 concentration on the photocatalytic activities of AgBr/WO_3.

AgBr content (Ag/W molar ratio)[a]	k_{app} (min^{-1})	Catalyst amount (g/L) [b]	k_{app} (min^{-1})	Initial MO concentration (mg/L)[c]	k_{app} (min^{-1})	Light intensity (lx)[d]	k_{app} (min^{-1})	H_2O_2 concentration (mmol/L)[e]	k_{app} (min^{-1})
0.05	0.0017	0.5	0.0041	5	0.0416	6000	0.0080	0	0.0057
0.10	0.0048	1.0	0.0069	10	0.0140	7000	0.0111	0.001	0.0060
0.15	0.0057	2.0	0.0160	15	0.0056	12000	0.0135	0.010	0.0074
0.20	0.0080	3.0	0.0184	20	0.0026	15000	0.0137	0.020	0.0079
0.25	0.0114	4.0	0.0216	25	0.0021	–	–	0.050	0.0067
0.30	0.0160	–	–	–	–	–	–	0.100	0.0062
0.40	0.0140	–	–	–	–	–	–	–	–

[a] 6000 lx of light intensity, 50 mL of suspension, 10 mg/L of initial MO concentration and 2.0 g/L of catalyst amount.
[b] Catalyst TF-0.30, 6000 lx of light intensity, 50 mL of suspension and 10 mg/L of initial MO concentration.
[c] Catalyst TF-0.30, 6000 lx of light intensity, 50 mL of suspension and 2.0 g/L of catalyst amount.
[d] Catalyst TD-0.20, 50 mL of suspension, 10 mg/L of initial MO concentration and 2.0 g/L of catalyst amount.
[e] Catalyst TC-0.15, 6000 lx of light intensity, 50 mL of suspension, 10 mg/L of initial MO concentration and 2.0 g/L of catalyst amount.

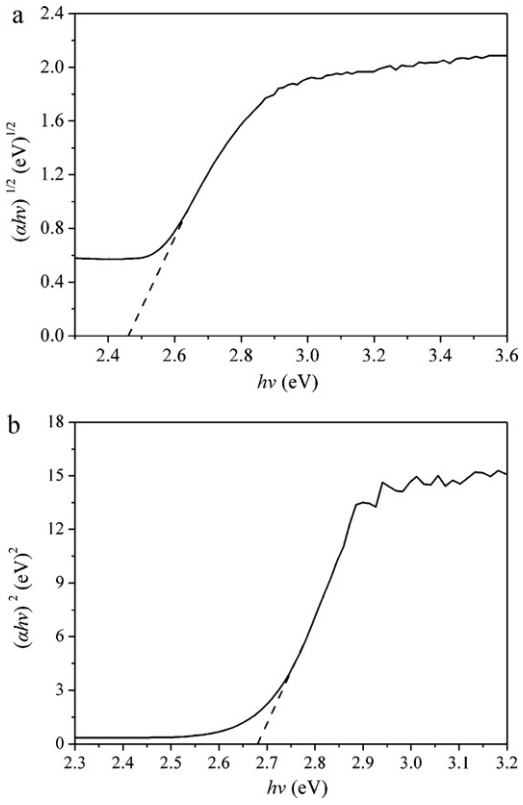

Fig. 4. Plots of (a) $(\alpha h\nu)^{1/2}$ versus energy ($h\nu$) for AgBr and (b) $(\alpha h\nu)^2$ versus energy ($h\nu$) for WO_3.

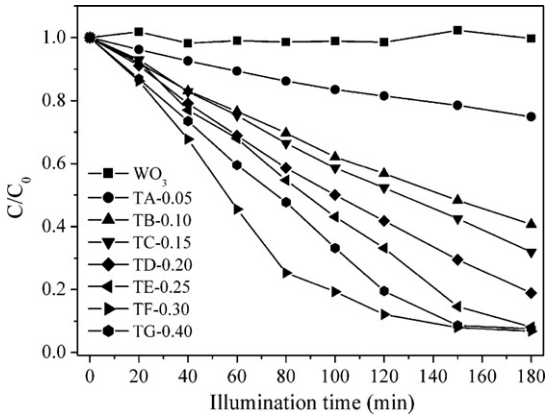

Fig. 5. Effect of AgBr content in catalysts on MO degradation during complete degradation process (6000 lx of light intensity, 50 mL of suspension, 10 mg/L of initial MO concentration and 2.0 g/L of catalyst amount).

activity decreased slightly, suggesting that the optimal AgBr content in AgBr/WO_3 existed when the molar ratio of Ag/W was 0.30:1 (catalyst TF-0.30). The degradation efficiency of MO was enhanced from 25.1% to 93.3% and remained unchanged after irradiation for 180 min with increasing AgBr content. Moreover, according to L–H kinetics model, the k_{app} of AgBr/WO_3 from TA-0.05 to TG-0.40 were respectively calculated and displayed in Table 1. The results clearly demonstrate the optimum AgBr content was 0.30 with the maximal degradation rate of 0.0160 min^{-1}. In AgBr/WO_3 system, only AgBr is the active component that absorbs visible light to initiate the photocatalytic reaction, so the AgBr content determines the number of electron-hole pairs that participate in the degradation of MO.

3.2.2. Effect of AgBr/WO_3 amount

Photocatalyst amount is one of critical parameters to the degradation efficiency of dyes. The amount of catalyst TF-0.30 changed from 0.5 to 4.0 g/L, and the corresponding k_{app} of MO degradation was shown in Table 1. The degradation efficiency of MO was enhanced with increasing catalyst amount and arrived highest k_{app} of 0.0216 min^{-1} at 4.0 g/L. k_{app} is not linear with catalyst amount but tends to remain almost constant at the higher catalyst amount because dye degradation is influenced by the active site and the photoabsorption of the catalyst [1]. Higher AgBr/WO_3 content indicates more active sites that can absorb much more photons. However, excessive catalyst does not display distinctively positive effect on degradation of MO due to the reduction in the penetration of light and light scattering by catalyst [1].

3.2.3. Effect of initial MO concentration

The effect of MO concentration on its degradation efficiency was investigated in the presence of 2.0 g/L catalyst TF-0.30. Table 1 shows that the k_{app} of MO decreased from 0.0416 to 0.0021 min^{-1} with increasing initial MO concentration from 5 mg/L to 25 mg/L. The possible reason is the visible light screening effect of the dye. At high MO concentration, a significant amount of visible light may be absorbed not by AgBr/WO_3 catalyst but by MO molecules, so the high MO concentration shields the light absorption for AgBr/WO_3 catalyst and reduces the photocatalytic activity of AgBr/WO_3.

3.2.4. Effect of visible light intensity

Four levels of light intensity were selected by adjusting the distance between the Xe lamp and the surface of the reaction solution [55] in the presence of catalyst TD-0.20 to observe the effect of light intensity on MO degradation. The light intensity was in the range of 6000–15,000 lx and the corresponding results are shown in Table 1. Clearly, degradation efficiency of MO was improved till the maximum by increasing light intensity from 6000 to 12,000 lx. If the

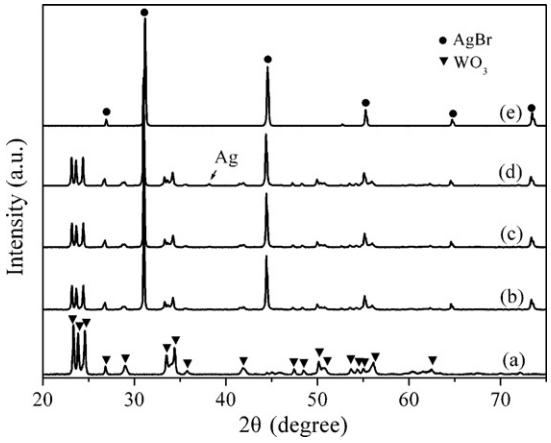

Fig. 6. XRD patterns of (a) WO_3, (b) the fresh TF-0.30, (c) the used TF-0.30 after degradation of MO under visible light for 60 min, (d) the used TF-0.30 after 7th cycling experiment and (e) AgBr.

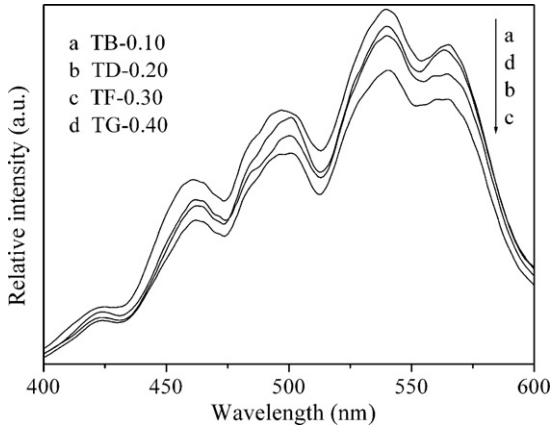

Fig. 7. Fluorescence emission spectra of $AgBr/WO_3$ samples with different AgBr content: (a) TB-0.10, (b) TD-0.20, (c) TF-0.30 and (d) TG-0.40.

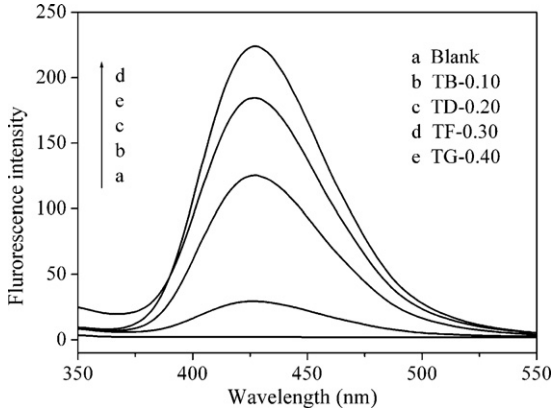

Fig. 8. PL spectra of $AgBr/WO_3$ sample in TA solution: (a) blank, (b) TB-0.10, (c) TD-0.20, (d) TF-0.30 and (e) TG-0.40 (each sample was illuminated for 60 min of visible light).

intensity was further increased to 15,000 lx, the k_{app} of MO was almost the same as that of 12,000 lx. Increasing the light intensity is beneficial to the absorption of photons for catalyst and the formation of electron-hole pairs, therefore the degradation efficiency of MO is increased. However, the quantity of AgBr on the surface of catalyst is limited while photons are present in excess amount [23], which may result in the waste of photons in the photocatalytic process.

In summary, the highest k_{app} of MO degradation can be obtained by controlling the influencing factors, in which AgBr content, $AgBr/WO_3$ amount and initial MO concentration exerted greater effects than the light intensity.

3.2.5. Stability of the catalyst

The catalyst's lifetime is an important parameter of the photocatalytic process, so it is essential to evaluate the stability of the catalyst for practical application. The photocatalytic process was repeated 7 times with catalyst TF-0.30 under visible light irradiation. The results show that the photocatalytic activity of $AgBr/WO_3$ declined quickly and the corresponding degradation efficiency of MO was 62.9%, 55.0%, 50.6%, 43.4%, 42.8%, 39.7% and 39.0%, respectively for each run. The recovered catalyst became a little darker than the newly prepared catalyst, which indicates that metal silver was formed in the used $AgBr/WO_3$. The XRD patterns of used $AgBr/WO_3$ are shown in Fig. 6. A small silver peak is found in 38.16° (JCPDS 04-0783) whereas the crystal structures of AgBr is well maintained. However, the trace amount of silver has affected the photocatalytic activity of $AgBr/WO_3$. This phenomenon has also been observed in previous studies [23,31,32]. Further experiments should be carried out to improve the stability of $AgBr/WO_3$.

3.3. Mechanism of MO photodegradation

3.3.1. Fluorescence emission spectra

It is known that the recombination of electron-hole can release energy in the form of fluorescence emission. Lower fluorescence emission intensity implies lower electron-hole recombination rate and high photocatalytic activity [56,57]. Using an ultraviolet light with 260 nm wavelength as excitation source, the fluorescence emission spectra of $AgBr/WO_3$ with different AgBr contents are shown in Fig. 7. It can be seen that the intensity of $AgBr/WO_3$ decreased from TB-0.10 to TF-0.30, and then increased up to TG-0.40, in which TF-0.30 displayed the lowest intensity of emission spectra. It indicates that TF-0.30 has the lowest electron-hole recombination rate, suggesting that the electrons and holes have longer lifetime and may form higher amount of active •OH. This is consistent with the highest photocatalytic activity of TF-0.30 observed. $AgBr/WO_3$ photocatalysts with other AgBr contents had correspondingly lower photocatalytic activity.

3.3.2. Hydroxyl radical analysis

According to the photocatalytic mechanism [19], a portion of photogenerated electrons and holes react with adsorbed oxygen/water to form different active species, such as hydroxyl radicals (•OH) that further involve in the dye oxidation process. The •OH radicals produced in water can be detected by PL or other techniques [49]. The formed •OH radicals on the surface of $AgBr/WO_3$ illuminated by visible light were detected by PL technique with terephthalic acid (TA) as a probe molecule in this study.

The PL emission spectra excited at 315 nm from TA solution suspension with $AgBr/WO_3$ were measured after each sample was illuminated for 60 min of visible light and the results are shown in Fig. 8. It can be seen that a PL signal was observed at 425 nm for each $AgBr/WO_3$ sample. The PL intensity was enhanced to maximum (TF-0.30) and then declined with increasing AgBr content. This suggests that the fluorescence is caused by chemical reactions of TA with •OH formed in photocatalytic reactions [49,50]. Hence •OH is the active species in $AgBr/WO_3$ system and finally induces the degradation of MO. Moreover, TF-0.30 catalyst produced the more active •OH than other samples, with maximal photocatalytic activity, which is also consistent with the results of fluorescence emission spectra (Fig. 7). The previous studies report that active •OH can be observed with

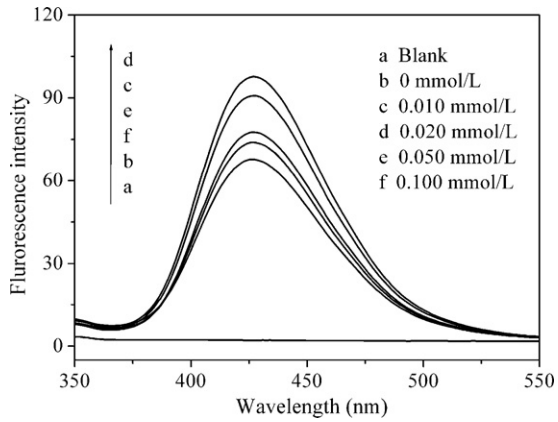

Fig. 9. PL spectral changes with H_2O_2 concentration: (a) blank, (b) 0 mmol/L, (c) 0.005 mmol/L, (d) 0.020 mmol/L, (e) 0.050 mmol/L and (f) 0.100 mmol/L (each sample was illuminated for 60 min of visible light).

electron spin resonance (ESR) technique for the AgX composite catalysts in the dye oxidation process [19,20,25,28,29]. Our result further provides the evidence of •OH formation for AgX composite catalysts under visible light.

In photocatalytic reaction, H_2O_2 is usually used as an electron acceptor to prevent the electron-hole pairs recombination and further improve the activity of catalyst. In this study, different concentration of H_2O_2 was added in AgBr/WO_3 system (TC-0.15) and the results are shown in Table 1. After adding a small amount of H_2O_2 (up to 0.020 mmol/L) the k_{app} increased from 0.0057 to 0.0079 min^{-1}, but if the H_2O_2 concentration was larger than 0.020 mmol/L, the k_{app} dropped to 0.0062 min^{-1} with the concentration of H_2O_2 at 0.100 mmol/L. A similar observation has been reported for other organic pollutants [58–60]. As a reference in this study, single H_2O_2 without TC-0.15 system did not show any degradation effect for MO.

The relevant PL emission spectra of AgBr/WO_3 system (TC-0.15) with different concentration of H_2O_2 were investigated and presented in Fig. 9. The trend of intensity change of •OH was the same as that of photocatalytic activity of AgBr/WO_3 with H_2O_2 addition. The amount of •OH is not consecutively increased with increasing H_2O_2 concentration while a maximal value appeared at 0.020 mmol/L H_2O_2. Comparatively, no PL signal at 425 nm was observed without AgBr/WO_3, which indicates that H_2O_2 could not decompose to •OH under visible light. This result further suggests that H_2O_2 acts as electron acceptor and takes part in the active •OH formation in the photocatalytic process.

Based on the results, a possible mechanism for the degradation of MO using AgBr/WO_3 system is proposed here: after AgBr/WO_3 absorbs the photons, both AgBr and WO_3 can be simultaneously excited to form electron-hole pairs. Subsequently photogenerated electrons transfer from the CB of AgBr to that of WO_3 and then convert to active •OH according to the following 4 steps [32]:

$$e^- + O_2 \rightarrow {}^\bullet O_2^- \quad (4)$$

$${}^\bullet O_2^- + H^+ \rightarrow {}^\bullet OOH \quad (5)$$

$${}^\bullet OOH + H^+ + e^- \rightarrow H_2O_2 \quad (6)$$

$$H_2O_2 + e^- \rightarrow {}^\bullet OH + OH^- \quad (7)$$

At the same time photogenerated holes also move in the opposite direction from the VB of AgBr/WO_3 to that of AgBr and also converted to active •OH in the light of 2 steps [62]:

$$h^+ + H_2O \rightarrow {}^\bullet OH + H^+ \quad (8)$$

$$h^+ + OH^- \rightarrow {}^\bullet OH \quad (9)$$

Consequently, active •OH results in the decomposition of MO under visible light by using AgBr/WO_3 system. In this process, the electron-hole pairs are separated efficiently, which further improves the photocatalytic activity of AgBr/WO_3.

At lower H_2O_2 amount, according to Eq. (7), additional H_2O_2 reacts with electrons to form more •OH and further enhance photocatalytic activity of AgBr/WO_3, while excess H_2O_2 also scavenge •OH to generate weaker oxidant $HO_2^\bullet$, H_2O and O_2 to depress photocatalytic activity of AgBr/WO_3, according to the following 2 steps [61]:

$$H_2O_2 + {}^\bullet OH \rightarrow HO_2^\bullet + H_2O \quad (10)$$

$$HO_2^\bullet + {}^\bullet OH \rightarrow H_2O + O_2 \quad (11)$$

4. Conclusions

The composite photocatalyst AgBr/WO_3 with AgBr on the surface of WO_3 substrate was prepared by simple deposition–precipitation method. AgBr/WO_3 exhibited good absorption in the visible light region. The photocatalytic activities of AgBr/WO_3 were differently affected by AgBr content in the catalyst, AgBr/WO_3 amount, initial MO concentration and light intensity. AgBr/WO_3 (TF-0.30) displayed the highest photocatalytic activity with k_{app} of 0.0160 min^{-1} under visible light, which coincided with the lowest intensity of fluorescence emission spectra and highest PL intensity of •OH formed in aqueous AgBr/WO_3 suspension. The photocatalytic activity of AgBr/WO_3 declined through cycling experiments due to the formation of trace amount of silver.

Acknowledgements

This work was financially supported by the Natural Science Foundation of China (No. 20973071) and Anhui Key Laboratory of Energetic Materials (No. KLEM2009013).

References

[1] R. Jiang, H.Y. Zhu, X.D. Li, L. Xiao, Visible light photocatalytic decolourization of C. I. Acid Red 66 by chitosan capped CdS composite nanoparticles, Chem. Eng. J. 152 (2009) 537–542.
[2] W.Z. Wang, W. Zhu, H.L. Xu, Monodisperse, mesoporous $Zn_xCd_{1-x}S$ nanoparticles as stable visible-light-driven photocatalysts, J. Phys. Chem. C 112 (2008) 16754–16758.
[3] S.C. Yan, Z.S. Li, Z.G. Zou, Photodegradation performance of g-C_3N_4 fabricated by directly heating melamine, Langmuir 25 (2009) 10397–10401.
[4] J.S. Jang, K.Y. Yoon, X.Y. Xiao, F.R.F. Fan, A.J. Bard, Development of a potential Fe_2O_3-based photocatalyst thin film for water oxidation by scanning electrochemical microscopy: effects of Ag–Fe_2O_3 nanocomposite and Sn doping, Chem. Mater. 21 (2009) 4803–4810.
[5] K. Ikeue, S. Shiiba, M. Machida, Novel visible-light-driven photocatalyst based on Mn–Cd–S for efficient H_2 evolution, Chem. Mater. 22 (2010) 743–745.
[6] R. Abe, H. Takami, N. Murakami, B. Ohtani, Pristine simple oxides as visible light driven photocatalysts: highly efficient decomposition of organic compounds over platinum-loaded tungsten oxide, J. Am. Chem. Soc. 130 (2008) 7780–7781.
[7] W. Zhao, W.H. Ma, C.C. Chen, J.C. Zhao, Z.G. Shuai, Efficient degradation of toxic organic pollutants with $Ni_2O_3/TiO_{2-x}B_x$ under visible irradiation, J. Am. Chem. Soc. 126 (2004) 4782–4783.
[8] J.C. Yu, W.K. Ho, J.G. Yu, H.Y. Yip, P.K. Wong, J.C. Zhao, Efficient visible-light-induced photocatalytic disinfection on sulfur-doped nanocrystalline titania, Environ. Sci. Technol. 39 (2005) 1175–1179.
[9] W. Ho, J.C. Yu, S.C. Lee, Low-temperature hydrothermal synthesis of S-doped TiO_2 with visible light photocatalytic activity, J. Solid State Chem. 179 (2006) 1171–1176.
[10] Q. Sun, Y.M. Xu, Sensitization of TiO_2 with aluminum phthalocyanine: factors influencing the efficiency for chlorophenol degradation in water under visible light, J. Phys. Chem. C 113 (2009) 12387–12394.
[11] I.M. Arabatzis, T. Stergiopoulos, M.C. Bernard, D. Labou, S.G. Neophytides, P. Falaras, Silver modified titanium dioxide thin films for efficient photodegradation of methyl orange, Appl. Catal. B: Environ. 42 (2003) 187–201.
[12] Y. Ishibai, J. Sato, T. Nishikawa, S. Miyagishi, Synthesis of visible-light active TiO_2 photocatalyst with Pt-modification: role of TiO_2 substrate for high photocatalytic activity, Appl. Catal. B: Environ. 79 (2008) 117–121.

[13] G.S. Li, D.Q. Zhang, J.C. Yu, Ordered mesoporous $BiVO_4$ through anocasting: a superior visible light-driven photocatalyst, Chem. Mater. 20 (2008) 3983–3992.
[14] J.W. Tang, Z.G. Zou, J.H. Ye, Effects of substituting Sr^{2+} and Ba^{2+} for Ca^{2+} on the structural properties and photocatalytic behaviors of $CaIn_2O_4$, Chem. Mater. 16 (2004) 1644–1649.
[15] D. Yamasita, T. Takata, M. Hara, J.N. Kondo, K. Domen, Recent progress of visible-light-driven heterogeneous photocatalysts for overall water splitting, Solid State Ionics 172 (2004) 591–595.
[16] R. Shi, J. Lin, Y.J. Wang, J. Xu, Y.F. Zhu, Visible-light photocatalytic degradation of $BiTaO_4$ photocatalyst and mechanism of photocorrosion suppression, J. Phys. Chem. C 114 (2010) 6472–6477.
[17] G.P. Li, J. Li, Y.J. Luo, AgBr nanoclusters: preparation by PAMAM dendrimers as template and photocatalytic property, Chin. J. Inorg. Chem. 23 (2007) 253–257.
[18] N. Kakuta, N. Goto, H. Ohkita, T. Mizushima, Silver bromide as a photocatalyst for hydrogen generation from CH_3OH/H_2O solution, J. Phys. Chem. B 103 (1999) 517–519.
[19] C. Hu, Y.Q. Lan, J.H. Qu, X.X. Hu, A.M. Wang, $Ag/AgBr/TiO_2$ visible light photocatalyst for destruction of azodyes and bacteria, J. Phys. Chem. B 110 (2006) 4066–4072.
[20] C. Hu, X.X. Hu, L.S. Wang, J.H. Qu, A.M. Wang, Visible-light-induced photocatalytic degradation of azodyes in aqueous AgI/TiO_2 dispersion, Environ. Sci. Technol. 40 (2006) 7903–7907.
[21] Y.Q. Lan, C. Hu, X.X. Hu, A.M. Wang, Efficient destruction of pathogenic bacteria with $AgBr/TiO_2$ under visible light irradiation, Appl. Catal. B: Environ. 73 (2007) 354–360.
[22] M.R. Elahifard, S. Rahimnejad, S. Haghighi, M.R. Gholami, Apatite-coated $Ag/AgBr/TiO_2$ visible-light photocatalyst for destruction of bacteria, J. Am. Chem. Soc. 129 (2007) 9552–9553.
[23] Y.J. Zang, F. Ramin, Photocatalytic activity of $AgBr/TiO_2$ in water under simulated sunlight irradiation, Appl. Catal. B: Environ. 79 (2008) 334–340.
[24] J. Cao, H.H. Lin, L. Jia, S.F. Chen, $AgBr/TiO_2$ composite catalyst: preparation by double-jet method and visible light photocatalytic property, Imaging Sci. Photochem. 27 (2009) 462–468.
[25] C. Hu, J. Guo, J.H. Qu, X.X. Hu, Photocatalytic degradation of pathogenic bacteria with AgI/TiO_2 under visible light irradiation, Langmuir 23 (2007) 4982–4987.
[26] Y.Z. Li, H. Zhang, Z.M. Guo, J.J. Han, X.J. Zhao, Q.N. Zhao, S.J. Kim, Highly efficient visible-light-induced photocatalytic activity of nanostructured AgI/TiO_2 photocatalyst, Langmuir 24 (2008) 8351–8357.
[27] Y. Yamashita, N. Aoyama, N. Takezawa, K. Yoshida, Characterization of hightly active $AgCl/Al_2O_3$ catalyst for photocatalytic conversion of NO, Environ. Sci. Technol. 34 (2000) 5211–5214.
[28] X.F. Zhou, C. Hu, X.X. Hu, T.W. Peng, J.H. Qu, Plasmon-assisted degradation of toxic pollutions with $Ag–AgBr/Al_2O_3$ under visible-light irradiation, J. Phys. Chem. C 114 (2010) 2746–2750.
[29] C. Hu, T.W. Peng, X.X. Hu, Y.L. Nie, X.F. Zhou, J.H. Qu, H. He, Plasmon-induced photodegradation of toxic pollutions with $Ag–AgI/Al_2O_3$ under visible-light irradiation, J. Am. Chem. Soc. 132 (2010) 857–862.
[30] S. Rodrigues, S. Uma, I.N. Martyanov, K.J. Klabunde, AgBr/Al-MCM-41 visible-light photocatalyst for gas-phase decomposition of CH_3CHO, J. Catal. 233 (2005) 405–410.
[31] Y.J. Zang, R. Farnood, J. Currie, Photocatalytic activities of AgBr/Y-zeolite in water under visible light irradiation, Chem. Eng. Sci. 64 (2009) 2881–2886.
[32] G.T. Li, K.H. Wong, X.W. Zhang, C. Hu, J.C. Yu, R.C.Y. Chan, P.K. Wong, Degradation of Acid Orange 7 using magnetic AgBr under visible light: the roles of oxidizing species, Chemosphere 76 (2009) 1185–1191.
[33] H.F. Cheng, B.B. Huang, Y. Dai, X.Y. Qin, X.Y. Zhang, One-step synthesis of nanostructured AgI/BiOI composite with highly enhanced visible-light photocatalytic performances, Langmuir 26 (2010) 6618–6624.
[34] P. Wang, B.B. Huang, X.Y. Zhang, X.Y. Qin, Y. Dai, H. Jin, J.Y. Wei, M.H. Whangbo, Composite semiconductor $H_2WO_4 \cdot H_2O$/AgCl as an efficient and stable photocatalyst under visible light, Chem. Eur. J. 14 (2008) 10543–10546.
[35] P. Wang, B.B. Huang, X.Y. Qin, X.Y. Zhang, Y. Dai, M.H. Whangbo, $Ag/AgBr/WO_3 \cdot H_2O$: visible-light photocatalyst for bacteria destruction, Inorg. Chem. 48 (2009) 10697–10702.
[36] L.S. Zhang, K.H. Wong, Z.G. Chen, J.C. Yu, J.C. Zhao, C. Hu, C.Y. Chan, P.K. Wong, $AgBr–Ag–Br_2WO_6$ nanojunction system: a novel and efficient photocatalyst with double visible-light active components, Appl. Catal. A: Gen. 363 (2009) 211–229.
[37] L.S. Zhang, K.H. Wong, H.Y. Yip, C. Hu, J.C. Yu, C.Y. Chan, P.K. Wong, Effective photocatalytic disinfection of E. coli K-12 using $AgBr–Ag–Bi_2WO_6$ nanojunction system irradiated by visible light: the role of diffusing hydroxyl radicals, Environ. Sci. Technol. 44 (2010) 1392–1398.
[38] M.A. Gondal, M.A. Dastageer, A. Khalil, Synthesis of nano-WO_3 and its catalytic activity for enhanced antimicrobial process for water purification using laser induced photo-catalysis, Catal. Commun. 11 (2009) 214–219.
[39] R.H. Victora, Calculated electronic structure of silver halide crystals, Phys. Rev. B 56 (1997) 4417–4421.
[40] X. Zhang, L.Z. Zhang, T.F. Xie, D.J. Wang, Low-temperature synthesis and high visible-light-induced photocatalytic activity of $BiOI/TiO_2$ heterostructures, J. Phys. Chem. C 113 (2009) 7371–7378.
[41] X.F. Chang, G. Yu, J. Huang, Z. Li, S.F. Zhu, P.F. Yu, C. Cheng, S.B. Deng, G.B. Ji, Enhancement of photocatalytic activity over $NaBiO_3/BiOCl$ composite prepared by an in situ formation strategy, Catal. Today 153 (2010) 193–199.
[42] W.Z. Yi, W.Z. Wang, L. Zhou, S.M. Sun, L. Zhang, CTAB-assisted synthesis of monoclinic $BiVO_4$ photocatalyst and its highly efficient degradation of organic dye under visible-light irradiation, J. Hazard. Mater. 173 (2010) 194–199.
[43] X. Dong, W. Ding, X. Zhang, X. Liang, Mechanism and kinetics model of degradation of synthetic dyes by $UV–vis/H_2O_2$/freeioxallate complexes, Dye Pigments 74 (2007) 470–476.
[44] S.F. Chen, X.L. Yu, W. Liu, Preparation and photocatalytic activity evaluation of composite photocatalyst $Fe–TiO_2/TiO_2$, ECS Trans. 21 (2009) 3–22.
[45] S.F. Chen, W. Zhao, W. Liu, H.Y. Zhang, X.L. Yu, Y.H. Chen, Preparation, characterization and activity evaluation of p–n junction photocatalyst p-$CaFe_2O_4$/n-Ag_3VO_4 under visible light irradiation, J. Hazard. Mater. 172 (2009) 1415–1423.
[46] Y. Li, X. Li, J. Li, J. Yin, Photocatalytic degradation of methyl orange by TiO_2-coated activated carbon and kinetic study, Water. Res. 40 (2006) 1119–1126.
[47] J.H. Sun, X.L. Wang, J.Y. Sun, R.X. Sun, S.P. Sun, L.P. Qiao, Photocatalytic degradation and kinetics of Orange G using nano-sized $Sn(IV)/TiO_2$/AC photocatalyst, J. Mol. Catal. A: Chem. 260 (2006) 241–246.
[48] C. Wu, H. Chang, J. Chen, Basic dye decomposition kinetics in a photocatalytic slurry reactor, J. Hazard. Mater. 137 (2006) 336–343.
[49] K. Ishibashi, A. Fujishima, T. Watanabe, K. Hashimoto, Detection of active oxidative species TiO_2 photocatalysis using the fluorescence technique, Electrochem. Commun. 2 (2000) 207–210.
[50] Q. Xiao, Z.C. Si, J. Zhang, C. Xiao, X.K. Tan, Photoinduced hydroxyl radical and photocatalytic activity of samarium-doped TiO_2 nanocrystalline, J. Hazard. Mater. 150 (2008) 62–67.
[51] H.M. Khan, M. Anwar, G.J. Ahmad, Effect of temperature and light on the response of an aqueous coumarin dosimeter, Radioanal. Nucl. Chem. Lett. 200 (1995) 521–527.
[52] X. Fang, G. Mark, C. Sonntag, OH radical formation by ultrasound in aqueous solutions part I: the chemistry underlying the terephthalate dosimeter, Ultrason. Sonochem. 3 (1996) 57–63.
[53] G.M. Makrigiorgos, J. Baranowska-Kortylewicz, E. Bump, S.K. Sahu, R.M. Berman, A.I. Kassis, A method for detection of hydroxyl radicals in the vicinity of biomolecules using radiation-induced fluorescence of coumarin, Int. J. Radiat. Biol. 63 (1993) 445–458.
[54] M. Galceran, M.C. Pujol, C. Zaldo, F. Daz, M. Aguil, Synthesis, structural, and optical properties in monoclinic Er:KYb$(WO_4)_2$ nanocrystals, J. Phys. Chem. C 113 (2009) 15497–15506.
[55] F.N. Chen, X.D. Yang, Q. Wu, Photocatalytic oxidation of *Escherischia coli*, *Aspergillus niger*, and formaldehyde under different ultraviolet irradiation conditions, Environ. Sci. Technol. 43 (2009) 4606–4611.
[56] T.J. Cai, M. Yue, X.W. Wang, Q. Deng, Preparation, characterization, and photocatalytic performance of $NdPW_{12}O_{40}/TiO_2$ composite catalyst, Chin. J. Catal. 28 (2007) 10–16.
[57] H. Tang, K. Prasad, R. Sanjines, P.E. Schmid, F. Levy, Electrical and optical properties of TiO_2 anatase thin films, J. Appl. Phys. 75 (1994) 2042–2047.
[58] C.M. So, M.Y. Cheng, J.C. Yu, P.K. Wong, Degradation of azo dye procion Red MX-5B by photocatalytic oxidation, Chemosphere 46 (2002) 905–912.
[59] S.F. Chen, G.Y. Cao, The effects of H_2O_2, metal ions on the photocatalytic reduction of Cr(VI) and photocatalytic oxidation of dichlorvos, Photogr. Sci. Photochem. 20 (2002) 435–440.
[60] W. Chu, C.C. Wong, The photocatalytic degradation of dicamba in TiO_2 suspensions with the help of hydrogen peroxide by different near UV irradiations, Water Res. 38 (2004) 1037–1043.
[61] W. Liu, S.F. Chen, W. Zhao, S.J. Zhang, Study on the photocatalytic degradation of trichlorfon in suspension of titanium oxide, Desalination 249 (2009) 1288–1293.